

DOI: 10.1002/elan.201700633

# Electrochemical Characterization and Electrocatalytic Application of Gold Nanoparticles Synthesized with Different Stabilizing Agents

Paulina Sierra-Rosales,<sup>\*[a]</sup> Rodrigo Torres,<sup>[b]</sup> Carlos Sepúlveda,<sup>[b]</sup> Marcelo J. Kogan,<sup>[b, c]</sup> and Juan Arturo Squella<sup>[d]</sup>

**Abstract:** Gold nanoparticles (AuNPs) have unique properties, making them attractive for electronic and energy-conversion devices and as (electro)catalysts for electrochemical sensors. In addition to the size and shape of AuNPs, the electrocatalytic properties of AuNP-sensors are also determined by the stabilizing agent used in their synthesis. Here, AuNPs were synthesized with citrate, alginate and quercetin, obtaining spherical and negatively charged nanoparticles. The AuNPs were used to modify glassy carbon electrodes (AuNPs/GCE), which were characterized by scanning electron microscopy and electrochemical techniques. The AuNPs/GCE showed aggregates of different sizes and degrees of dispersion on the electrode surface depending on the stabilizing agent. The

AuNP's aggregates affect the homogeneity of the film, the reproducibility of the electrodes and their response in buffer solution. Finally, to evaluate the electrocatalytic ability of the AuNPs/GCE, we studied the oxidation of two analytes with opposite charges: (1) sunset yellow (negative) and (2) hydrazine (positive). Compared with GCE, the AuNPs/GCE showed good electrocatalytic properties for hydrazine, increasing the current up to 50% and shifting the potential by almost 400 mV, depending on the AuNP used. For the negatively charged analyte, the current decreased up to 50% and no shift in potential was observed. Thus, the electrocatalytic properties of the AuNPs showed to be highly dependent on the nature of the analyte.

**Keywords:** Gold nanoparticles • stabilizing agent • electrocatalysis • hydrazine • sunset yellow

## 1 Introduction

At present, it is well known that the use of nanomaterials for electrode modification increase their surface area which improve the sensitivity of the electrochemical (bio)sensor. Therefore, a nanomaterial-modified electrode has a variety of potential applications including catalysis, chemical and biological sensing, energy-conversion devices, etc. [1–6]. In this context the most used nanomaterials nowadays are carbon derivatives (carbon nanotubes (CNT), graphene oxide (GO), etc.) [7–10], metallic nanoparticles (MNPs) (e.g., gold, silver, copper) [11–14] and their hybrids (MNPs/CNT, MNPs/GO, etc.) [15–21]. Gold nanoparticles have attracted enormous interest due their electronic, optical, catalytic and magnetic properties [12,22,23]. In addition, AuNPs improve the electron transfer and enhance the analytical sensitivity [16,14]. The disadvantage of using AuNPs it is that their electrocatalytic properties depend on their size and shape [16,24–26]; therefore, the route of synthesis of the AuNPs and the method of immobilization on the electrode surface must be controlled.

The AuNP-modified electrodes are usually fabricated by electrochemical deposition of the nanoparticles from the auric acid solution ( $HAuCl_4$ ) [15,27–29], by immersion of the electrode in a colloidal gold solution (dip-coating) [30–32] or by casting a certain volume of colloidal gold solution on the surface of the electrode (drop-

coating) [33–35]. The electrodeposition of nanoparticles is one of the most used methods to modify electrodes because the attachment of the AuNPs favors the direct communication with the electrode. However, the electrolysis reaction does not tend to proceed uniformly, hence the deposition conditions (potential and time) and the concentration of  $AuCl_4^-$  must be controlled [23]. Usually the size of the AuNPs electrodeposited is higher than

[a] P. Sierra-Rosales

Programa Institucional de Fomento a la Investigación, Desarrollo e Innovación, Universidad Tecnológica Metropolitana, Ignacio Valdivieso 2409, P.O. Box 8940577, San Joaquín, Santiago, Chile

E-mail: psierra@utem.cl

[b] R. Torres, C. Sepúlveda, M. J. Kogan


Departamento de Química Farmacológica y Toxicológica, Facultad de Ciencias Químicas y Farmacéuticas, Universidad de Chile. 8380492, Santiago, Chile

[c] M. J. Kogan

Advanced Center for Chronic Diseases (ACCDiS), Santiago, Chile

[d] J. Arturo Squella

Departamento de Química Orgánica y Físicoquímica, Facultad de Ciencias Químicas y Farmacéuticas, Universidad de Chile. 8380492, Santiago, Chile

 Supporting information for this article is available on the WWW under <https://doi.org/10.1002/elan.201700633>

those chemically prepared; thereby, the modification of the electrode with colloidal gold nanoparticles allows working with AuNPs with a well-controlled shape and size, compared with electrodeposition [26, 29, 33, 36].

The most used synthetic route to obtain colloidal gold nanoparticles is the *in-situ* Turkevich-Frens method with citrate, obtaining spherical and negatively charged nanoparticles [37]. The main drawback of this method is the low stability of the AuNPs obtained [38]. Other synthetic procedure includes thiolate-stabilized AuNPs that used  $\text{NaBH}_4$  as reducing agent (B Brust-Schiffrin method). The size of the AuNPs synthesized by this method is much smaller than that obtained by Turkevich-Frens, and the Au-sulfur bond between the thiolate and the AuNPs is stronger than the bond formed between Au-citrate. The withdrawal of the common synthetic routes (including citrate, borohydride or other organic compounds) is that they may be associated with environmental toxicity or biological hazards [39]. Some previous studies have introduced a green method using natural polymers and flavonoids. Quercetin is the most abundantly consumed bio-flavonoid, highly concentrated in tea, apple and onion [40]. It exhibits antioxidant and anti-inflammatory properties and can act as stabilizing and reducing agent for AuNPs [40–42]. Alginate, the main constituent of brown algae, is a well-known biopolymer and belongs to a polysaccharide family. Sodium alginate is known as a stabilizer and template for synthesis of metal nanoparticles [39, 43]. The advantage of using quercetin and alginate as reducing/stabilizing agents is that both are biocompatible and nontoxic [38–40, 43].

During the design of electrochemical sensors, the main concern about colloidal AuNPs is that the stabilizing agent may interfere with the electron-transfer reactions and may affect the electrocatalytic properties of the AuNPs. For example, thiol capping is too strong to obtain good electrochemical results limiting its applications [23]. The adequate selection of the stabilizing agent will determine its suitability as an electrocatalyst. Therefore, it is important to evaluate the role of the stabilizing agent in the performance of AuNP-modified electrodes as candidates for future electrochemical applications.

The aim of this work is to investigate the effect of the stabilizing agent of the AuNPs on their electrocatalytic properties. Here, the AuNPs were synthesized separately with citrate, quercetin (bioflavonoid) and alginate (natural polysaccharide) as stabilizing/reducing. The AuNPs synthesized have the same shape and average size of the metallic center, low poly dispersity indexes and negative charges; therefore, any change in their electrocatalytic response could be associated to the stabilizing agent used. The AuNPs-modified glassy carbon electrodes were prepared by drop-coating and the electrocatalytic effect of the AuNPs was evaluated by studying the oxidation of analytes with opposite charges.

## 2 Experimental

### 2.1 Reagents

Gold(III) chloride trihydrate ( $\text{HAuCl}_4 \times 3\text{H}_2\text{O}$ ) (CAS 16961–25-4), sodium citrate tribasic dihydrate ( $\text{C}_6\text{H}_5\text{Na}_3\text{O}_7 \times 2\text{H}_2\text{O}$ ) (CAS 6132–04-3), quercetin (2-(3,4-dihydroxyphenyl)-3,5,7-trihydroxy-4H-1-benzopyran-4-one, 3,3',4',5,6-pentahydroxyflavone) (CAS 117-39-5), potassium ferricyanide(III) ( $\text{K}_3[\text{Fe}(\text{CN})_6]$ ) (CAS 13746-66-2), potassium hexacyanoferrate(II) trihydrate ( $\text{K}_4[\text{Fe}(\text{CN})_6] \times 3\text{H}_2\text{O}$ ) (CAS 14459-95-1), hexaamineruthenium(III) chloride ( $\text{Ru}(\text{NH}_3)_6\text{Cl}_3$ ) (CAS 14282-91-8), sunset yellow (CAS 2783-94-0) and hydrazine dihydrochloride ( $\text{N}_2\text{H}_4 \times 2\text{HCl}$ ) (CAS 5341-61-7) were purchased from Sigma-Aldrich. NaOH was from Merck-Chile. Alginate was extracted from brown seaweed (*Desarestia menziessi*) [44] and characterized in the Universidad de Santiago de Chile. The solutions were prepared with ultrapure water (Milli-Q, Millipore System Inc.). The electrochemical experiments were conducted in phosphate-buffered saline (0.1 M PBS, pH 7.0) as the supporting electrolyte solution.

### 2.2 Preparation of Colloidal Gold Nanoparticles with Different Stabilizing Agents

#### 2.2.1 Citrate-coated Gold Nanoparticles (AuNP-CT)

AuNP-CT were prepared by citrate reduction of  $\text{HAuCl}_4$  as described previously [45, 46]. Briefly, an aqueous solution of  $\text{HAuCl}_4$  (100 mL, 1 mM) was refluxed for 5–10 min and a warm (50–60 °C) aqueous solution of sodium citrate (10 mL, 38.8 mM) was quickly added. The reflux was continued for another 30 min until a deep red solution was obtained. The solution was passed through 0.45  $\mu\text{m}$  Millipore syringe filters to remove any precipitate, the pH was adjusted to 7.4 using a dilute NaOH solution and the filtrate was stored at 4 °C.

#### 2.2.2 Quercetin-coated Gold Nanoparticles (AuNP-QC)

3.02 mg of quercetin were dissolved in NaOH (2 mL, 10 mM) and dilute to a final volume of 10 mL in a flask protected from light. In a round-bottom flask  $\text{HAuCl}_4$  (1 mL, 1 mM) was mixed with distilled water (8 mL) with continuous stirring. Then, quercetin (1 mL, 1 mM) freshly prepared was added drop wise. The solution was protected from light and stirred at room temperature for 2 h. The prepared aqueous quercetin-nanoparticles (AuNP-QC) were passed through a membrane filter (0.22  $\mu\text{m}$ ) and centrifuged at 16168 g for 30 min. The pelleted were resuspended in water (10 mL) and stored at 4 °C.

#### 2.2.3 Alginate-coated Gold Nanoparticles (AuNP-AG)

AuNPs-AG was prepared mixing solutions of sodium alginate (0.5  $\text{mg mL}^{-1}$ ) and  $\text{HAuCl}_4$  (1 mM) with stirring in a bath at 70 °C. The pH was adjusted to 11.0 using a

0.1 M NaOH. The reaction was carried out during 1 hour until the color of the solution changes from yellow pale to pink, characteristic of gold colloidal solutions. The AuNP-AG was stored at 4 °C.

### 2.3 Characterization of AuNPs

The surface plasmon resonance peak of the AuNPs was achieved by a Lambda 25 UV/VIS spectrophotometer (PerkinElmer Inc.). Nanoparticle surface charges were measured using a Malvern Zetasizer Nano-ZS (Malvern Instruments). Measurements were performed in 1.2 mM sodium citrate at pH 7.4. pH was adjusted with 1.0 M HCl or with 1.0 M NaOH, at 25 °C, in a 3-mm light path cuvette. The measurements were conducted with a disposable 301 polycarbonate capillary cell (DTS 1061, Malvern) under precise temperature control (25 °C). Because the zeta potential measurements were performed in an aqueous solution, the Smoluchowski approximation was used to calculate the zeta potential from the measured electrophoretic mobility. DLS measurements were obtained at 25 °C in a 3 mm light path cuvette. The refractive index was considered 1.4. The nanoparticles diameter and morphology were obtained using a scanning transmission electron microscope (STEM) Model F50 Inspect (FEI Company). The sample was prepared by dropping the AuNP on formvar carbon-coated copper microgrids and allowing them to dry. For the scanning electron microscopy (SEM) measurements we used a glassy carbon disk (TED Pella brand, INC (N° 16524), 12.7 mm diameter). The disks were cleaned by polishing with 0.3 and 0.05 µm alumina slurries before modification. Then, 5 µL of the AuNPs were casting onto the disk surface and dried at room temperature for 45 min. The morphologies of the modified disks were investigated by SEM using an Inspect Scanning Electron Microscope F50 operated at 10 kV.

The stability of AuNPs was studied following the UV-vis spectra after storage the AuNPs for at least one month at 4 °C. After that time, the absorbance of the solutions were recorded and compared with those obtained at the moment of the synthesis.

### 2.4 Preparation of AuNPs-modified Glassy Carbon Electrode (AuNPs/GCE)

Before modification, the GCE was polished with 0.3 and 0.05 µm alumina slurries for 1 min and then washed thoroughly with water. Subsequently, 5 µL of the AuNPs were casting onto the GCE surface and dried at room temperature for 45 min. The resulting electrode was denoted as AuNPs/GCE.

### 2.5 Electrochemical Measurements

Cyclic voltammetry (CV) and differential pulse voltammetry (DPV) were performed on a CHI 650 setup (CH Instruments Inc., USA). A conventional three-electrode system was used with a GCE (Model CHI 104, CH

Instruments Inc.) or AuNPs-modified GCE as the working electrode; a platinum wire (BASiMW-1032) and Ag/AgCl (3.0 M NaCl, Model RE-5B, BAS) as the counter and reference electrode, respectively. All potentials are given relative to the reference electrode. A magnetic stirrer provided convective transport when necessary.

Electrochemical measurements of AuNPs/GCE were carried out in 0.1 M PBS at pH 7.0. Cyclic voltammograms (CV) and differential pulse voltammograms (DPV) were performed over the potential range of 0.0 V–1.2 V. The DPV operating conditions were a potential increment of 0.004 V, pulse amplitude of 0.05 V and pulse period of 0.2 s. All experiments were conducted at room temperature and in triplicate.

## 3 Results and Discussion

### 3.1 Characterization of Colloidal Gold Nanoparticles (AuNPs)

AuNPs were synthesized with three different stabilizing agents: citrate (CT), quercetin (QC) and alginate (AG). Then, these AuNPs were characterized by UV-visible, scanning transmission electron microscopy (STEM), dynamic light scattering (DLS) and zeta potential, results shown in Figure 1 and summarized in Table 1.

Table 1. Physicochemical characterization of gold nanoparticles.

AuNP	SPB/ nm	Size by STEM/nm	Size by DLS/nm	PDI	Z potential /mV
AuNP- CT	519±2	12.0±1.7	23.2±1.0	0.4	-45.4±2.3
AuNP- QC	522±5	11.6±8.3	18.1±1.5	0.5	-45.0±3.5
AuNP- AG	523±1	12.5±1.7	19.4±2.1	0.4	-62.2±3.7

AuNP, gold nanoparticles; CT, citrate; QC, quercetin; AG, alginate; SPB, surface Plasmon band; STEM, scanning transmission electron microscopy; DLS, dynamic light scattering; PDI, poly dispersity index.

In Figure 1, the spectrophotometric measurement showed a narrow absorption peak close to 520 nm (519±2, 520±5 and 523±1 nm for AuNP-CT, AuNP-QC and AuNP-AG, respectively); which is attributed to AuNPs with a diameter of approximately 12 nm [41, 46, 47].

The STEM images showed small and spherical AuNPs, independently of the stabilizing agent used. The size distribution was evaluated statistically by measuring the diameter of 100 AuNPs in the STEM images. The average particle size is estimated to be about 12 nm (12.0±1.7, 11.6±8.3 and 12.5±1.7 nm for AuNP-CT, AuNP-QC and AuNP-AG, respectively), which is in agreement with surface plasmon bands observed by UV-visible.

The hydrodynamic diameter of the AuNPs obtained from the DLS method was closed to 20.2±2.65 nm with a



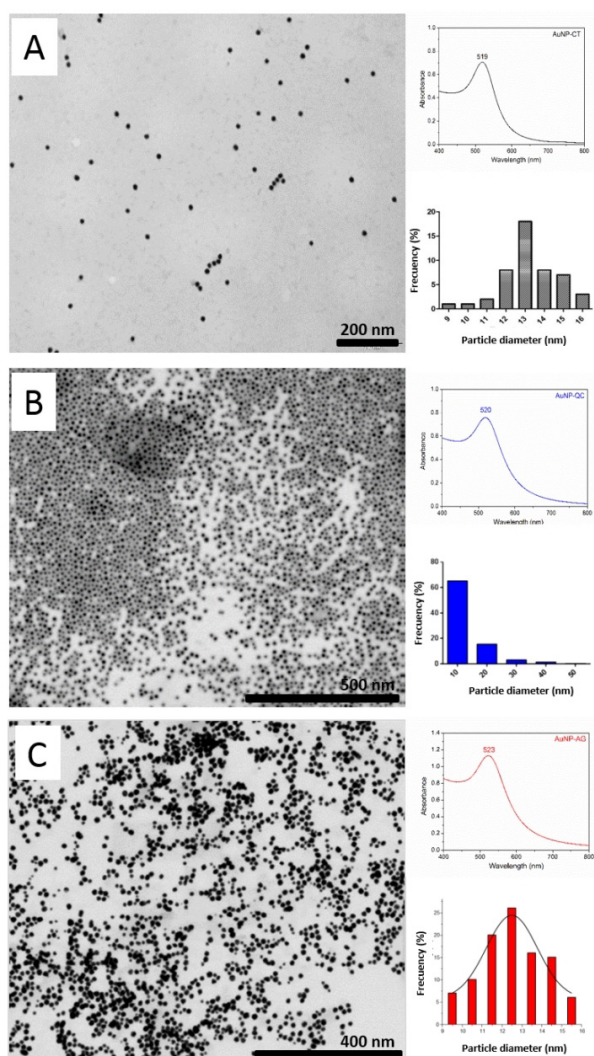


Fig. 1. STEM images, size distribution histograms and UV-vis absorption spectra of AuNPs synthesized with different stabilizing agents. (A) citrate-coated AuNP, (B) quercetin-coated AuNP and (C) alginate-coated AuNP.

poly dispersity index of 0.4, suggesting that the stabilizing agents makes a coating on the nanoparticles. This method was also used to measure the charge of the surface (zeta potential). In this case, the AuNPs obtained with citrate and quercetin showed an average zeta potential of  $-45$  mV, meanwhile the zeta potential of the AuNPs synthesized with alginate was  $-62$  mV. In all cases, the negative charges will increase the electrostatic repulsion between nanoparticles, which will prevent the particle aggregation. The complete characterization of the AuNPs is summarized in Table 1.

To determine the stability of the AuNPs, the aqueous solutions were kept at  $4^{\circ}\text{C}$  for 30 days, after which the UV-vis spectra were recorded and compared with the spectra measured at the moment of the synthesis. For all the AuNPs, after 30 days of storage the UV-vis spectra did not show changes in the surface plasmon band (SBP)

compared to the day of the synthesis (not shown here). This result is in agreement with other reports under the same storage conditions [38,48].

### 3.2 Surface Characterization of AuNPs Deposited onto a Glassy Carbon Electrode (AuNP/GCE)

The modification of the electrode was performed by placing a small volume of the colloidal gold solution on the surface and allowed to dry at room temperature for 45 minutes. Figure 2 shows the SEM images of AuNPs with different stabilizing agents deposited onto a GCE at two different magnifications. The AuNPs correspond to the bright spots meanwhile the black background is the GC disk surface, similar to what was observed by Gotti et al. [33].

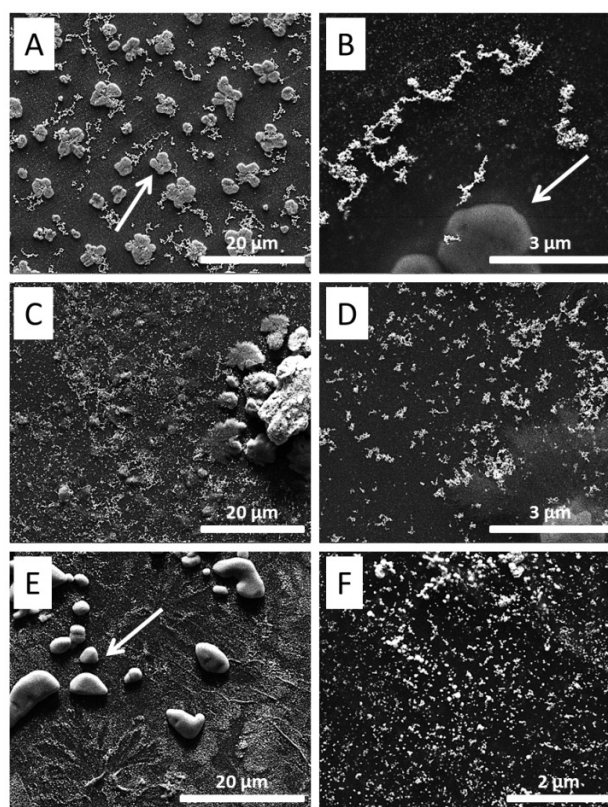


Fig. 2. SEM images of AuNP-modified glassy carbon electrodes: (A–B) AuNP-CT/GCE, (C–D) AuNP-QC/GCE and (E–F) AuNP-AG/GCE at different magnifications.

For AuNP-CT (Figure 2A–B) the nanoparticles are observed as bright chains due to the formation of aggregates. The gray clover-like structures (size  $\sim 5$   $\mu\text{M}$ ) observed in Figure 2A (see white arrow) correspond to sodium citrate crystals. Similarly, Gotti et al. [33] observed white aggregates in the SEM images, corresponding to sodium chloride crystals.

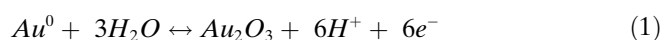
With higher magnification, the morphology of the AuNP-CT aggregates is well defined; while the citrate

crystals are less clear (at the bottom of the image). The formation of aggregates by AuNP-CT can be explained due to the weak nature of the Au-citrate bond [37]. As the electrode is dried, the Au-citrate bond loses stability and the nanoparticles start to interact between them and aggregate. When the stabilizing agent is quercetin (Figure 2C–D) the size of the AuNP-QC aggregates is smaller but they are better distributed than AuNP-CT, indicating that the interaction between quercetin-AuNP is stronger than for citrate-AuNP. Finally, AuNP-AG (Figure 2E–F) were distributed on the surface homogeneously in the form of bright and round-shaped particles. It is known that the use of polymers as stabilizing agents enhance the stability of the AuNP, explaining the observed behavior [37]. The big structures observed in Figure 2E (see white arrow) are most probably alginate deposits.

The result shows that despite the different colloidal AuNPs had the same size for the metallic center (Table 1), after letting them dry on the electrode these form different aggregates depending on the stabilizing agent used. In this case, the best deposit in terms of homogeneity corresponded to the AuNP synthesized with alginate, which prevents the aggregation of the nanoparticles unlike citrate. These aggregates affect the homogeneity of the film, which is an important issue in the construction of an electrochemical sensor.

### 3.3 Electrochemical Characterization of AuNPs/GCE

Figure 3A shows the electrochemical profile of a glassy carbon electrode (GCE) and a solid gold electrode (AuE) in 0.1 M PBS (pH 7.0). GCE does not show faradaic processes in the entire potential window used, which is not the case for the AuE. In that case an anodic peak close to 0.90 V is observed attributed to the formation of Au oxides, which are reduced on the backward scan given a reduction peak close to 0.480 V. Figure 3B shows the cyclic voltammograms of AuNPs/GCE in 0.1 M PBS (pH 7.0). For AuNP-CT/GCE and AuNP-QC/GCE the cyclic voltammetric profiles show the typical shape of Au electrochemical activation. A broad peak between 0.90 and 1.0 V corresponds to the oxidation of the AuNPs and the formation of a metal oxide. The cathodic peak close to 0.45 V in the reverse scan is related to the reduction of the gold oxides (Eq. 1) [49]. This experiment is commonly used to confirm the electrodeposition or the attachment of AuNPs [27, 30, 33, 50–52].



For AuNP-CT/GCE the redox peaks observed have the highest charge (Q) compared to AuNP-QC/GCE and AuNP-AG/GCE. But, when the stabilizing agent is alginate the electrode behaves like GCE and the redox pair associated with the gold reduction-oxidation process is not observed. The electrochemical parameters of these electrodes are summarized in Table 2.

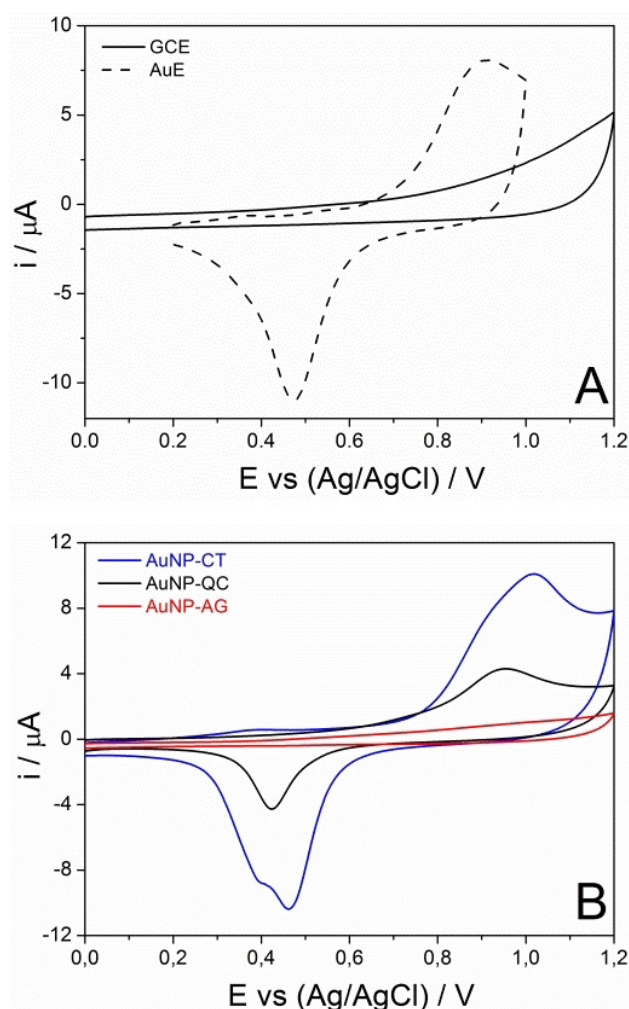


Fig. 3. Cyclic voltammograms in 0.1 M PBS (pH 7.0): (A) Bare glassy carbon and gold electrodes and (B) AuNPs-modified GCE. Scan rate: 50 mVs<sup>-1</sup>.

Table 2. Electrochemical parameters of electrodes in 0.1 M PBS (pH 7.0) obtained from Figure 3.

Electrode	E <sub>p,c</sub> /mV	Q/μC
AuE	474	9.66
GCE	–	–
AuNP-CT/GCE	462	8.93
AuNP-QC/GCE	424	3.50
AuNP-AG/GCE	–	–

E<sub>p,c</sub>, cathodic peak potential; Q, charge associated to E<sub>p,c</sub>.

These results show that AuNP-CT/GCE formed a film with more gold exposed to the electrolyte solution showing a voltammetric profile similar to a bare gold electrode (Figure 3A). This is in good agreement with the aggregates observed by SEM (Figure 2). The size of the aggregates formed by AuNP-QC and visualized through SEM is smaller than the observed for AuNP-CT, and the charge (Q) of the cathodic peak of AuNP-QC/GCE is 60% smaller than AuNP-CT/GCE. For AuNP-AG/GCE



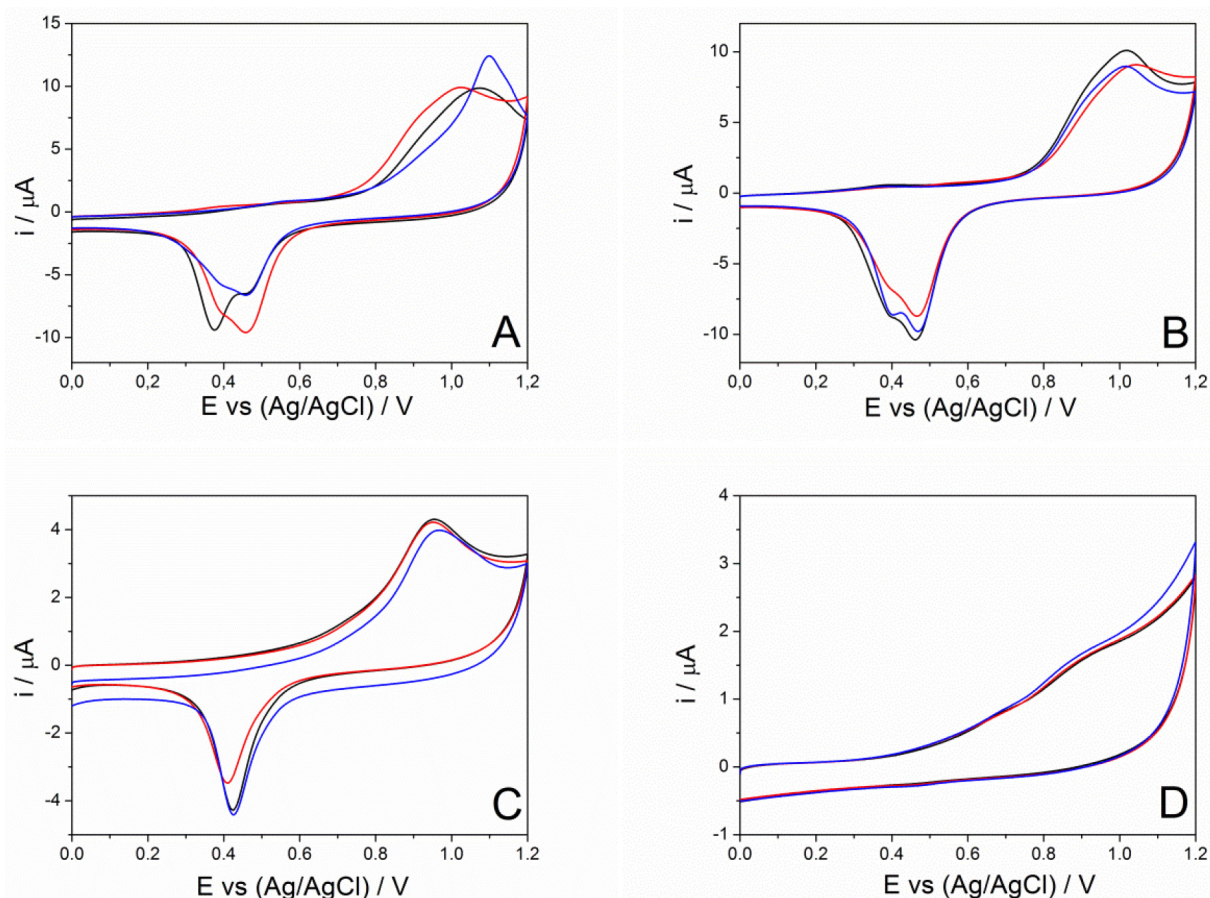


Fig. 4. Cyclic voltammograms of AuNPs/GCE in 0.1 M PBS (pH 7.0): (A) AuNP-CT/GCE dried in oven at 50 °C for 15 minutes, (B) AuNP-CT/GCE dried at room temperature (r.t.) for 45 minutes, (C) AuNP-QC/GCE dried at r.t. for 45 minutes and (D) AuNP-AG/GCE dried at r.t. for 45 minutes. Scan rate: 50 mV s<sup>-1</sup>.

the voltammetric profile does not show redox processes. This is probably because the alginate avoids the generation of aggregates and it homogeneously covers the AuNPs, which blocks the redox active surface from the AuNP and thus no redox process is detected. The charge values in Table 2 are comparable with those previously reported for AuNPs electrodeposited [25] and for AuNPs deposited by drop-coating on GCE [33]. These values varied between 0.2 and 11.9  $\mu\text{C}$ , depending on the methodology used for the modification of the electrode. According to Gotti et al. [33], highest Q values suggest a higher active surface area. In our case the active surface area follows the order AuNP-AG < AuNP-QC < AuNP-CT.

In order to improve the modification process of the electrodes, two procedures were evaluated: (1) to dry the electrode at room temperature and (2) to dry it in oven at 50 °C for 15 min (Figure 4A–B).

With both procedures AuNP-CT/GCE shows the oxidation and reduction of the AuNPs but when the electrode is dried in an oven the reproducibility diminishes. Even more, the cathodic peak changes in shape and intensity. Therefore, we choose the first method, which involves drying the electrode at room temperature. Even

though the time of preparation could seem to be long, compared with other experimental procedures, 45 minutes is the shortest time of preparation described at this date [26,30,32,33,53].

As can be seen from Figure 4B–D, the most reproducible electrode is AuNP-AG/GCE. This could be related to the high covering capability provided by the stabilizing agent, which decreases the interaction between nanoparticles and consequently the formation of aggregates allowing getting a more homogeneous film. That could be the reason why AuNP-AG/GCE shows less aggregates according to the SEM images and the voltammetric profile is the most reproducible.

### 3.4 Electrochemical Behavior of Redox Probes on AuNPs/GCE

The three stabilizing agents used in this work added negative charges to the surface of the nanoparticle. As it could be expected, the negative charges of the AuNPs may affect the response of the modified electrode against charges analytes. To determine this effect, we studied the electrochemical response of the AuNPs/GCE against two electroactive species with opposite charges,  $[\text{Fe}(\text{CN})_6]^{-3/-4}$

and  $[\text{Ru}(\text{NH}_3)_6]^{+3/+2}$ . Both redox mediators have a well-defined monoelectronic and reversible mechanism onto GCE. Thus, any change observed in the electrochemical parameters should be associated with the modification of the AuNPs-film.

Figure 5A shows the CV profile of 1.0 mM  $[\text{Fe}(\text{CN})_6]^{-3/-4}$  on GCE and AuNPs/GCE. For GCE, the peak-to-peak separation ( $\Delta E_p$ ) for  $[\text{Fe}(\text{CN})_6]^{-3/-4}$  corresponded to 70 mV at  $50 \text{ mV s}^{-1}$  (close to the theoretical value of  $59/n \text{ mV}$ , where  $n=1$ ) and a relationship between the backward and the forward peak currents ( $i_{p,c}/i_{p,a}$ ) of 0.99, i.e., the amount of redox mediator oxidized and reduced is almost the same. When the electrode is modified with AuNPs, a clear decrease in the current and an increase in the  $\Delta E_p$  were observed. The nanoparticles affect the electronic transfer making it more difficult, losing the reversibility of the couple. From Table 3, it is possible to appreciate that the ratio  $i_{p,c}/i_{p,a}$  kept unchanged, indicating that the same amount of redox mediator is reduced and oxidized. Also, from this table it is clear that the  $\Delta E_p$  decreases in the following order  $\text{AuNP-AG} < \text{AuNP-QC} < \text{AuNP-CT}$ . According to Table 2 that order follows the same trend observed for the active surface area. Consequently, AuNP-CT/GCE has the most heterogeneous film and the highest active surface area.

The aggregates of AuNP-CT could have low quantities of citrate, which reduced the negative charges on the surface; therefore, the effect on the electronic transfer is smaller. On the other hand, AuNP-QC and AuNP-AG formed more homogeneous films on the electrode, exposing less gold (active surface area) and incorporating more negative charges to the surface electrostatically repelling the redox mediator. This was reflected by the increase of the  $\Delta E_p$  values.

In the case of  $[\text{Ru}(\text{NH}_3)_6]^{+3/+2}$  (Figure 5B–C), the  $\Delta E_p$  observed on GCE, AuNP-CT/GCE and AuNP-QC/GCE kept unchanged, with values close to 60 mV (Table 3). This is indicative of a monoelectronic reversible mechanism and the ratio  $i_{p,a}/i_{p,c}$  slightly decreases compared with GCE but with values close to the unit. For AuNP-AG/GCE the  $\Delta E_p$  is reduced to 53 mV, demonstrating that the electron transfer process is improved due to the presence of the nanoparticle. The  $\Delta E_p$  value is lower than the theoretical value probably due to the adsorption of the mediator. The ratio  $i_{p,a}/i_{p,c}$  diminishes due to the fact that the cathodic peak is 90% higher than the anodic peak; thus, the amount of oxidized specie is higher than the reduced one at the beginning of the potential scan.

These results show that the response of the AuNP-modified electrode depends on the charge of the analyte. When the analyte is negatively charged as  $[\text{Fe}(\text{CN})_6]^{-3/-4}$ , it is electrostatically repelled by the AuNP deposited on the electrode, but when the analyte is positively charged as  $[\text{Ru}(\text{NH}_3)_6]^{+3/+2}$ , the electronic transfer between the analyte and the electrode is facilitated. This causes an increase in the sensitivity of the electrode.

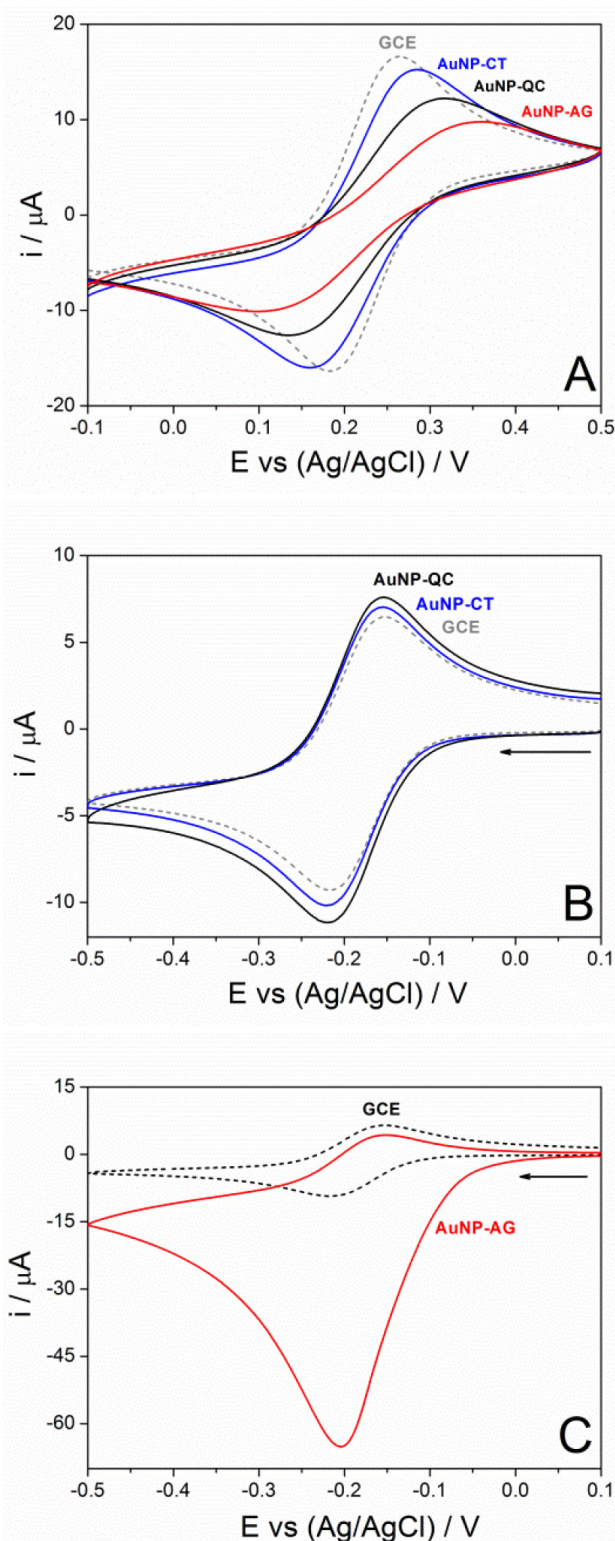


Fig. 5. Cyclic voltammograms of 1.0 mM of (A)  $[\text{Fe}(\text{CN})_6]^{-3/-4}$  and (B–C)  $[\text{Ru}(\text{NH}_3)_6]^{+3/+2}$  at GCE and AuNPs/GCE in 0.1 M PBS (pH 7.0). Scan rate:  $50 \text{ mV s}^{-1}$ .



Table 3. Electrochemical parameters of redox mediators obtained from Figure 5.

	$[\text{Fe}(\text{CN})_6]^{-3/-4}$		$[\text{Ru}(\text{NH}_3)_6]^{+3/+2}$	
	$i_{p,c}/i_{p,a}$	$\Delta E_p/\text{mV}$	$i_{p,a}/i_{p,c}$	$\Delta E_p/\text{mV}$
GCE	0.99	70	0.98	62
AuNP-CT/GCE	0.94	124	0.86	65
AuNP-QC/GCE	0.98	167	0.94	66
AuNP-AG/GCE	1.0	260	0.13	53

$i_{p,c}$ , cathodic peak current;  $i_{p,a}$ , anodic peak current;  $\Delta E_p$ , difference between the two peak potentials

### 3.5 Electrocatalytic Properties

To get deeper insights into the electrocatalytic performance of the modified-electrodes for applications with charged analytes, the DPV response of the bare GCE and AuNPs/GCE were compared for the electrooxidation of a negatively charged analyte (sunset yellow) and a positively charged analyte (hydrazine).

Figure 6A shows the differential pulse voltammetry (DPV) profiles of GCE and AuNPs/GCE in 0.1 M PBS (pH 7.0) in absence of analytes. In agreement with CV

responses (Figure 3B), AuNP-CT/GCE and AuNP-QC/GCE showed an oxidation process associated to the nanoparticle. On the other hand, AuNP-AG/GCE has a DPV similar to GCE due to the fully covering of the nanoparticle with the polymer.

Sunset yellow is a food dye negatively charged at pH 7.0 due to the presence of two sulfonate groups in its structure (Figure S1). This dye is oxidized at GCE and neutral media via  $1e^-/1H^+$  [2], showing a single peak close to 0.60 V. The oxidation of this analyte onto AuNPs/GCE did not show any shift in peak potentials and in a similar way of what was observed with  $[\text{Fe}(\text{CN})_6]^{-3/-4}$ , the presence of AuNPs did not improve the response of the bare electrode. Even more, the loss in the current is up to 50%.

Hydrazine ( $pK_a=8.23$  [54]), is oxidized mainly through  $4e^-/4H^+$  process, with  $\text{N}_2$  as the final product in aqueous solution [55,56]. Also, it is highly dependent on the surface structure of the electrode, which affects the electrocatalysis of the reaction [49,55]. In Figure 6B the DPVs were obtained in the presence of 1.0 mM hydrazine. For GCE, two broad signals were observed at 0.56 V and 1.00 V. These signals are overlapped, which difficult the quantification of hydrazine. When the electrode is

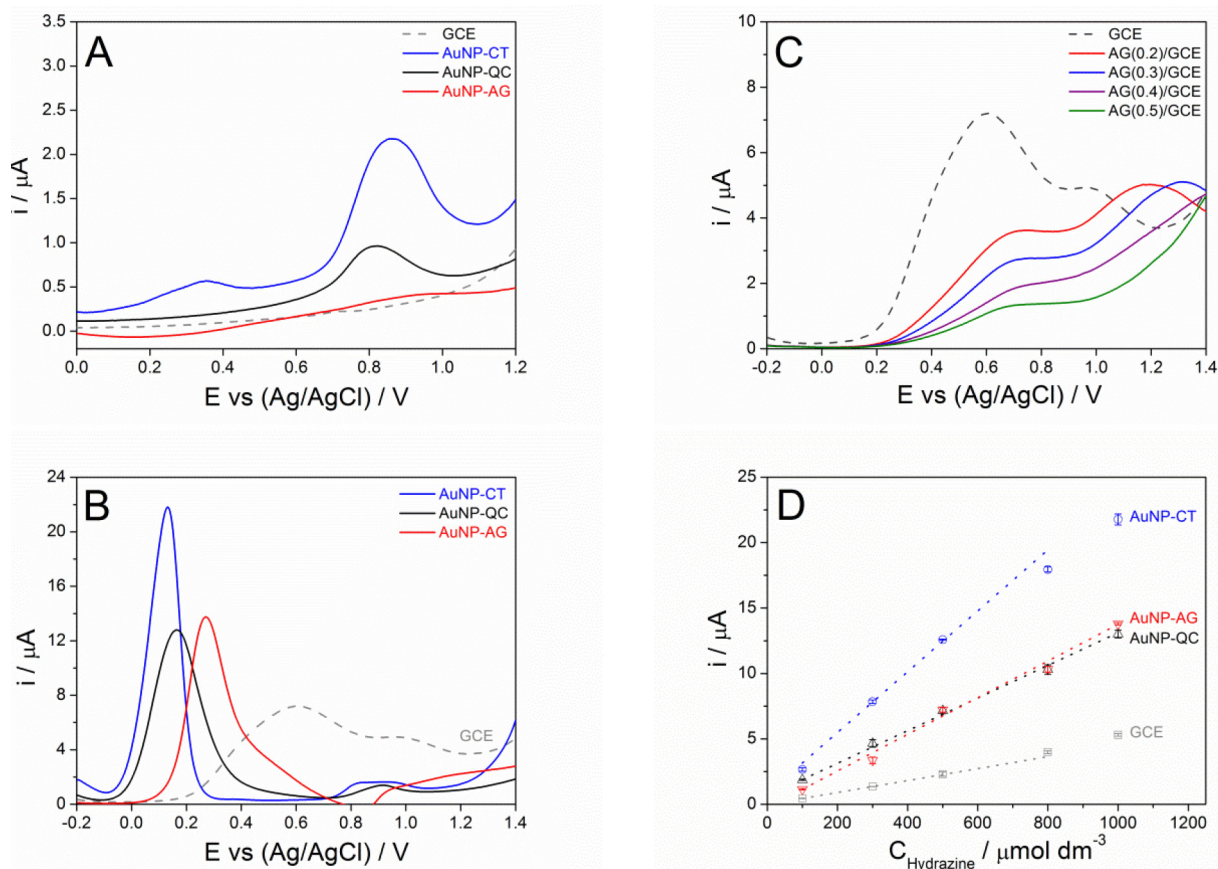


Fig. 6. (A) DPVs of AuNPs/GCE in absence of hydrazine in 0.1 M PBS (pH 7.0), (B) DPVs of AuNP/GCE in presence of 1.0 mM hydrazine in 0.1 M PBS (pH 7.0), (C) DPVs of 1.0 mM hydrazine in 0.1 M PBS (pH 7.0) at GCE modified with different concentrations of alginate (0.2, 0.3, 0.4 and 0.5  $\text{mg mL}^{-1}$ ), (D) peak current as a function of different concentrations of hydrazine.



modified with AuNPs, a narrow single peak is detected. In the case of AuNP-CT/GCE and AuNP-QC/GCE a second peak is observed close to 0.85 V due to the oxidation of the AuNP showed in Figure 6A. The oxidation of hydrazine onto AuNP-modified electrodes showed a shift to more negative values of the peak potential and an increase in the current values. These results indicate that the AuNPs electrocatalyze the oxidation of hydrazine and it is in agreement with other electrodes modified with AuNPs [49,57]. Good electrocatalytic properties of AuNP-CT has been also observed for other positively charged analytes like ractopamine and metaproterenol [34], in which case the authors associated the results with the electrostatic attraction between the AuNP and the analyte. For hydrazine, with AuNP-CT/GCE the current increases by 75% compared to GCE and the peak potential shifts to 0.13 V. For AuNP-QC/GCE, the current increase corresponds to 57% and the peak potential shifts to 0.16 V; and for AuNP-AG/GCE, the current increases by 62% and the peak potential appears in 0.22 V. Thus, the electrocatalysis observed in terms of shift potential follows the order AuNP-AG < AuNP-QC < AuNP-CT.

According to what was obtained for  $[\text{Ru}(\text{NH}_3)_6]^{+3/+2}$ , with hydrazine we expected that the best response would have been with AuNP-AG/GCE followed by AuNP-QC/GCE and then AuNP-CT/GCE. However, according to our results the best catalytic electrode in terms of shift potential and current value was AuNP-CT/GCE instead of AuNP-AG/GCE. This is similar to that observed by Koçak et al. [58]. Koçak electrodeposited AuNPs onto a poly-bromocresol/carbon nanotube-modified GCE and studied the effect of the  $\text{Au}^{+3}$  solution concentration on the peak current of hydrazine. According to those studies, as the gold concentration increases, the peak associated with the oxidation of hydrazine was shifted to more negative potentials and the peak current was increased. In agreement with those results our electrodes showed the following trend in terms of gold surface exposure and therefore, the active surface area: AuNP-AG < AuNP-QC < AuNP-CT (from Table 2); which is the same order for the electrocatalysis of hydrazine. In this case, the predominant interaction could be between the gold exposed and hydrazine over the electrostatic interaction between the hydrazine and the stabilizing agent of the AuNP.

As can be seen in the experimental section, for the synthesis of AuNP-AG the concentration of alginate used was  $0.5 \text{ mg mL}^{-1}$  and according to our results that value is enough to fully cover the AuNP. In order to prove if the amount of alginate (AG) is affecting the response of the electrode against the oxidation of hydrazine, we modified the glassy carbon electrode with different concentrations of the polymer (Figure 6C). When the concentration of AG increases from 0 to  $0.5 \text{ mg mL}^{-1}$ , the peak potential of hydrazine shift to more positive values (almost 100 mV), and the currents values decrease, where for  $0.5 \text{ mg mL}^{-1}$  the loss in current reach a 92%. These results prove that the presence of AG difficult the electronic transfer and

that the low catalytic effect for the oxidation of hydrazine with AuNP-AG/GCE is not only related with the stabilizing capability of the polymer and the homogeneity of the film.

Figure 6D shows the calibration plots for hydrazine in 0.1 M PBS (pH 7.0) and the analytical parameters were determined and compared with other AuNP-modified electrodes (table 4). The plot of the peak current versus concentration of hydrazine showed in Figure 6D present a linear correlation for GCE and AuNPs/GCE. Other authors showed two linear segments in the calibration plots, which were attributed to the generation of  $\text{N}_2$  on the electrode surface. The presence of the bubbles could changes the catalytic surface affecting the diffusion of the analyte to the electrode. In agreement of what was observed for Li et al. [59] at low hydrazine concentration, the formed  $\text{N}_2$  bubbles are little and may not block the diffusion of hydrazine from the bulk solution.

The reproducibility of the modified electrodes (RSD%) was less than 3% (2.3% for AuNP-CT/GCE and AuNP-AG/GCE, and 2.5% for AuNP-QC/GCE) showing high reproducibility of the electrodes at pH 7.0. Also, the limit of detection for all the AuNPs is comparable to other sensors (Table 4). All the AuNPs used in this work improve the sensitivity of the bare electrode. With respect to GCE, the AuNPs/GCE electrocatalyzes the oxidation of hydrazine showing good sensitivity and reproducibility. Compared with other electrodes with AuNPs, the analytical parameters such as limit of detection (LOD) and reproducibility are improved.

## 4 Conclusions

In the present work, we prepared AuNPs with three different stabilizing agents to modify a glassy carbon electrode. The implemented synthetic routes gave spherical and negatively charged nanoparticles of 12 nm of average size, where the colloidal nanoparticles were similar in shape, size and charge. After the modification of the electrodes, the formed films show different homogeneity depending on the stabilizing agent, and therefore, affecting the electrochemical response of the sensor. Electrodes with big aggregates, such as the obtained with AuNPs stabilized with citrate (AuNP-CT) showed a voltammetric profile similar to the corresponding to a solid gold electrode. On the contrary, when the film of AuNPs was more homogenous as the obtained with AuNPs stabilized with alginate (AuNP-AG), the voltammograms was similar to a bare GCE without redox processes and the reproducibility of the electrode was improved.

As the stabilizing agents are negatively charged, we assessed the effect of these charges on the electrocatalytic ability of the AuNPs-modified electrodes by studying the oxidation of analytes with positive and negative charges. When the analyte was negatively charged, the electrodes did not improve the response with respect to the bare

Table 4. Comparison of the analytical performances for hydrazine determination by using different modified electrodes.

Modified electrode	Method	pH	$E_p/V$	RSD/%	LOD/ $\mu M$	Sensitivity/ $\mu A \mu M^{-1}$	Linear range/ $\mu M$	Ref.
AuNP/MnO <sub>2</sub> /GCE	DPV	7.0	0.18	–	1.80	694 ( $\mu A mM^{-1} cm^{-2}$ )	5.0–2000	[60]
AuNP/GPE	SWV	5.0	0.28	6.0	0.04	$4.3 \times 10^{-4}$	0.05–1000	[30]
	Amperometry				3.1	$4.3 \times 10^{-6}$	25–1000	
Au/PPy/GCE	DPV	7.0	0.12	2.9	0.20	0.126	1–500	[59]
						0.036	500 - 7500	
AuNP/SWCNH/GCE	Amperometry	7.4	0.15	3.8	1.1	59.1	5.0–645	[36]
						36.1	645–3345	
AuNP/PDITYB/MWCNTs/GCE	CV	8.0	0.07	6.7	0.60	0.24	2.0–130	[50]
						0.14	130–350	
GCE	DPV	7.0	0.56	1.8	1.71	0.005	8.8–800	
AuNP-CT/GCE	DPV	7.0	0.13	2.3	0.41	0.023	3.9–800	This work
AuNP-QC/GCE	DPV	7.0	0.16	2.5	0.95	0.012	7.2–1000	
AuNP-AG/GCE	DPV	7.0	0.22	2.3	0.55	0.014	5.0–1000	

<sup>a</sup>Ag/AgCl 3.0 M; RSD, relative standard deviation; LOD, limit of detection; AuNP/MnO<sub>2</sub>/GCE, gold nanoparticle-MnO<sub>2</sub> modified glassy carbon electrode; DPV, differential pulse voltammetry; AuNP/GPE, gold nanoparticle-modified graphite pencil electrode; SWV, square wave voltammetry; Au/PPy/GCE, gold nanoparticle-polypyrrol nanowire modified glassy carbon electrode; AuNP/SWCNH/GCE, gold nanoparticles single walled carbon nanohorns-modified glassy carbon electrode; AuNP/PDITYB/MWCNTs/GCE, gold nanoparticles/poly(4,5-dihydro-1,3-thiazol-2-ylsulfanyl-3-methyl-1,2-benzenediol)/multiwalled carbon nanotubes-modified glassy carbon electrode; CV, cyclic voltammetry.

electrode, as it may be expected because of the electrostatic repulsion between the analyte and the stabilizing agent located at the AuNP surface. On the contrary, when the analyte was positively charged the electrodes show improved electrocatalytic properties and high reproducibility compared with the bare electrode. This was mostly associated to the electrostatic attraction between the analyte and the stabilizing agent, which facilitated the electron transfer. All the AuNPs used in this work improved the sensitivity of the bare electrode, increased the current values and shifted the oxidation potentials of hydrazine. Therefore, our results indicate that the electrocatalytic application of these electrodes is highly dependent on the charge of the analyte. Finally, a balance between the AuNP covering homogeneity to electrostatically attract the analyte towards the electrode, and the amount of gold active surface exposed for the electron transfer needs to be achieved to improve the electrocatalytic properties of AuNP-modified electrodes.

## Acknowledgements

This work was supported by FONDECYT 3140533, 3150515 and FONDAP 15130011

## References

- N. Jadon, R. Jain, S. Sharma, K. Singh, *Talanta* **2016**, *161*, 894–916.
- P. Sierra-Rosales, C. Toledo-Neira, J. A. Squella, *Sensors Actuators, B Chem.* **2017**, *240*, 1257–1264.
- Y. Zhang, Q. Wei, *J. Electroanal. Chem.* **2016**, *781*, 401–409.
- P. A. Rasheed, N. Sandhyarani, *Microchim. Acta* **2017**, *184*, 981–1000.
- M. L. Yola, T. Eren, N. Atar, H. Saral, I. Ermiş, *Electroanalysis* **2016**, *28*, 570–579.
- A. Tolga Çolak, T. Eren, M. L. Yola, E. Beşli, O. Şahin, N. Atar, *J. Electrochem. Soc.* **2016**, *163*, F1237–F1244.
- Y. Liu, X. Dong, P. Chen, *Chem. Soc. Rev.* **2012**, *41*, 2283–2307.
- Y. Wang, Y. Shao, D. W. Matson, J. Li, Y. Lin, *ACS Nano* **2010**, *4*, 1790–1798.
- Ö. A. Yokuş, F. Kardaş, O. Akyildirim, T. Eren, N. Atar, M. L. Yola, *Sensors Actuators, B Chem.* **2016**, *233*, 47–54.
- M. L. Yola, N. Atar, *J. Electrochem. Soc.* **2017**, *164*, B223–B229.
- K. Ghanbari, *Synth. Met.* **2014**, *195*, 234–240.
- F. W. Campbell, R. G. Compton, *Anal. Bioanal. Chem.* **2010**, *396*, 241–259.
- S. S. Narwade, B. B. Mulik, S. M. Mali, B. R. Sathe, *Appl. Surf. Sci.* **2017**, *396*, 939–944.
- M. L. Yola, N. Atar, T. Eren, H. Karimi-Maleh, S. Wang, *RSC Adv.* **2015**, *5*, 65953–65962.
- C. Saengsookwaow, R. Rangkupan, O. Chailapakul, N. Rodthongkum, *Sensors Actuators, B Chem.* **2016**, *227*, 524–532.
- M. L. Yola, N. Atar, *Electrochim. Acta* **2014**, *119*, 24–31.
- M. L. Yola, V. K. Gupta, T. Eren, A. E. Şen, N. Atar, *Electrochim. Acta* **2014**, *120*, 204–211.
- M. L. Yola, T. Eren, N. Atar, *Sensors Actuators, B Chem.* **2015**, *210*, 149–157.
- M. L. Yola, T. Eren, N. Atar, *Electrochim. Acta* **2014**, *125*, 38–47.
- M. L. Yola, N. Atar, *J. Electrochem. Soc.* **2016**, *163*, B718–B725.
- S. Elçin, M. L. Yola, T. Eren, B. Girgin, N. Atar, *Electroanalysis* **2016**, *28*, 611–619.
- K. Saha, S. S. Agasti, C. Kim, X. Li, V. M. Rotello, *Chem. Rev.* **2012**, *112*, 2739–2779.
- M. Oyama, *Anal. Sci.* **2010**, *26*, 1–12.
- H. Erikson, A. Sarapuu, K. Tammeveski, J. Solla-Gullón, J. M. Feliu, *ChemElectroChem* **2014**, *1*, 1338–1347.
- G. Gotti, K. Fajerberg, D. Evrard, P. Gros, *Electrochim. Acta* **2014**, *128*, 412–419.
- D. Geng, G. Lu, *J. Nanoparticle Res.* **2007**, *9*, 1145–1151.
- C. Karuppiah, S. Palanisamy, S. M. Chen, S. K. Ramaraj, P. Periakaruppan, *Electrochim. Acta* **2014**, *139*, 157–164.



- [28] R. Devasenathipathy, V. Mani, S. M. Chen, D. Arulraj, V. S. Vasantha, *Electrochim. Acta* **2014**, *135*, 260–269.
- [29] S. Koçak, B. Aslışen, *Sensors Actuators, B Chem.* **2014**, *196*, 610–618.
- [30] M. Abdul Aziz, A. N. Kawde, *Talanta* **2013**, *115*, 214–221.
- [31] A. R. Fakhari, H. Ahmar, H. Hosseini, S. Kazemi Movahed, *Sensors Actuators, B Chem.* **2015**, *213*, 82–91.
- [32] L. Zhang, X. Jiang, E. Wang, S. Dong, *Biosens. Bioelectron.* **2005**, *21*, 337–345.
- [33] G. Gotti, D. Evrard, K. Fajerwerg, P. Gros, *J. Solid State Electrochem.* **2016**, *20*, 1539–1550.
- [34] J. Duan, D. He, W. Wang, Y. Liu, H. Wu, Y. Wang, M. Fu, *Chem. Phys. Lett.* **2013**, *574*, 83–88.
- [35] S. Hajihosseini, N. Nasirizadeh, M. S. Hejazi, P. Yaghmaei, *Mater. Sci. Eng. C* **2016**, *61*, 506–515.
- [36] S. Zhao, L. Wang, T. Wang, Q. Han, S. Xu, *Appl. Surf. Sci.* **2016**, *369*, 36–42.
- [37] P. Zhao, N. Li, D. Astruc, *Coord. Chem. Rev.* **2013**, *257*, 638–665.
- [38] D. K. Das, A. Chakraborty, S. Bhattacharjee, S. Dey, *J. Exp. Nanosci.* **2013**, *8*, 649–655.
- [39] N. Tue Anh, D. Van Phu, N. Ngoc Duy, B. Duy Du, N. Quoc Hien, *Radiat. Phys. Chem.* **2010**, *79*, 405–408.
- [40] R. Pal, S. Panigrahi, D. Bhattacharyya, A. S. Chakraborti, *J. Mol. Struct.* **2013**, *1046*, 153–163.
- [41] K. A. Rawat, S. K. Kailasa, *Microchim. Acta* **2014**, *181*, 1917–1929.
- [42] L. A. Levchenko, S. A. Golovanova, N. V. Lariontseva, A. P. Sadkov, D. N. Voilov, Y. M. Shul'Ga, N. G. Nikitenko, A. F. Shestakov, *Russ. Chem. Bull.* **2011**, *60*, 426–433.
- [43] S. Saha, A. Pal, S. Kundu, S. Basu, T. Pal, *Langmuir* **2010**, *26*, 2885–2893.
- [44] F. Martínez-Gómez, A. Mansilla, B. Matsuhira, M. C. Matulewicz, M. A. Troncoso-Valenzuela, *Carbohydr. Polym.* **2016**, *146*, 90–101.
- [45] R. Prades, S. Guerrero, E. Araya, C. Molina, E. Salas, E. Zurita, J. Selva, G. Egea, C. López-Iglesias, M. Teixidó, *Biomaterials* **2012**, *33*, 7194–7205.
- [46] S. Guerrero, E. Araya, J. L. Fiedler, J. I. Arias, C. Adura, F. Albericio, E. Giralt, J. L. Arias, M. S. Fernández, M. J. Kogan, *Nanomedicine (Lond)*. **2010**, *5*, 897–913.
- [47] A. Pal, K. Esumi, T. Pal, *J. Colloid Interface Sci.* **2005**, *288*, 396–401.
- [48] S. K. Balasubramanian, L. Yang, L. L. Yung, C. Ong, W. Ong, *Biomaterials* **2010**, *31*, 9023–9030.
- [49] A. Celebanska, M. Opallo, *ChemElectroChem* **2016**, *3*, 1629–1634.
- [50] A. R. Fakhari, H. Ahmar, H. Hosseini, S. Kazemi Movahed, *Sensors Actuators, B Chem.* **2015**, *213*, 82–91.
- [51] G. Chang, H. Shu, K. Ji, M. Oyama, X. Liu, Y. He, *Appl. Surf. Sci.* **2014**, *288*, 524–529.
- [52] R. Huang, L. H. Guo, *Sci. China Chem.* **2010**, *53*, 1778–1783.
- [53] B. Jin, X. Ji, T. Nakamura, *Electrochim. Acta* **2004**, *50*, 1049–1055.
- [54] E. W. McCleskey, W. Almers, *Proc. Natl. Acad. Sci. U.S.A.* **1985**, *82*, 7149–7153.
- [55] R. Gisbert, A. Boronat-Gonzalez, J. M. Feliu, E. Herrero, *ChemElectroChem* **2017**, *4*, 1130–1134.
- [56] M. Mazloum-Ardakani, R. Mazidi, M. H. Mashhadizadeh, P. Rahimi, M. A. Karimi, *Sci. China Chem.* **2010**, *53*, 1195–1201.
- [57] G. Maduraiveeran, R. Ramaraj, *Electrochem. commun.* **2007**, *9*, 2051–2055.
- [58] S. Koçak, B. Aslışen, *Sensors Actuators, B Chem.* **2014**, *196*, 610–618.
- [59] J. Li, X. Lin, *Sensors Actuators, B Chem.* **2007**, *126*, 527–535.
- [60] M. Wang, W. Li, P. Hu, S. He, H. Yang, *Int. J. Electrochem. Sci.* **2016**, *11*, 1928–1937.

Received: October 12, 2017

Accepted: December 6, 2017

Published online on December 29, 2017